International Journal of Solids and Structures 49 (2012) 2582–2589

Contents lists available at SciVerse ScienceDirect

International Journal of Solids and Structures

journal homepage: www.elsevier.com/locate/ijsolstr

A constitutive equation for graphene based on density functional theory

Mei Xu [a], Jeffrey T. Paci [b,c,*], Jay Oswald [e], Ted Belytschko [d]

[a] Theoretical and Applied Mechanics, 2145 N. Sheridan Rd., Northwestern University, Evanston, IL 60208, USA
[b] Department of Chemistry, University of Victoria, Victoria, British Columbia, Canada V8W 3V6
[c] Department of Chemistry, 2145 N. Sheridan Rd., Northwestern University, Evanston, IL 60208, USA
[d] Department of Mechanical Engineering, 2145 N. Sheridan Rd., Northwestern University, Evanston, IL 60208, USA
[e] School for Engineering of Matter, Transport and Energy, Arizona State University, Tempe, AZ, USA

ARTICLE INFO

Article history:
Received 8 March 2011
Received in revised form 22 May 2012
Available online 1 June 2012

Keywords:
Graphene
Anisotropic
Elastic constants
Nanoindentation

ABSTRACT

An anisotropic strain energy function is proposed for tensile loading in graphene that provides a nonlinear, hyperelastic constitutive equation. In the proposed function, the energy depends on the principal invariants of the right Cauchy–Green tensor and the strains in the zigzag and armchair directions. The use of the zigzag and armchair strains gives the model the ability to account for anisotropic behavior at moderate deformations. The constitutive law parameters are determined by a least squares fit to the energies predicted by density functional theory (DFT) calculations, and a good match is obtained to the DFT results for zigzag and armchair graphene sheets with various loading combinations. The law is applied in a continuum calculation of nanoindentation of a graphene membrane. The force–deflection predicted with this model show excellent agreement with analogous experimental results, thus providing a strong link between DFT calculations and nanoexperiments.

1. Introduction

Quantum mechanics opens the possibility of developing constitutive equations for crystalline materials and, with time, even more complex materials. While mechanicians have so far relied on experiments to develop these equations, this approach is often limited, particularly for small crystals. By using quantum mechanics, the response of a crystal to various loadings can be obtained, and an accurate constitutive equation can be derived. In this paper, we develop such an equation for graphene by this approach. By means of a unit cell, we obtain the response to various loadings, and then develop a constitutive equation that fits closely our quantum–mechanical density functional theory (DFT) results.

Graphene is a two-dimensional form of carbon, consisting of a single layer of atoms in a hexagonal arrangement. Initially it was thought that such a crystal would be thermodynamically unstable and could not exist (Mermin, 1968). Early reports of the exfoliation of graphene layers from graphite suggested thicknesses of tens to hundreds of layers (Lu et al., 1999; Shioyama, 2001); the binding between the layers was assumed to be due to van der Waals forces. Recently, Novoselov and Geim and colleagues (Geim and Novoselov, 2007; Novoselov et al., 2005) invalidated the instability hypothesis and creating free-standing single layers using a micromechanical cleavage technique. This pioneering work drew considerable attention to this "newly-discovered" material. The high mechanical strength, excellent thermal conductivity, and unusual electrical properties of graphene present many opportunities for application in composite materials (Stankovich et al., 2006; Paci et al., 2007) and nanoelectronic devices (Li et al., 2008; Ohta et al., 2006; Sakhaee-Pour et al., 2008; Stoller et al., 2008), and have led to the creation of a large body of related scientific work.

The successful isolation of graphene sheets was quickly followed by many laboratory studies. Frank et al. (2007) measured the effective spring constants of stacks of graphene sheets up to five layers by the atomic force microscopy deflection measurements. The first experimental measurement of the mechanical properties of a single layer was made by Lee et al. (2008). They measured the deflection at the center point of the graphene sheets in nanoindentation experiments, and obtained distributions of the Young's modulus. Assuming a graphene thickness 0.335 nm, the resulting modulus is 1.0 ± 0.1 TPa.

The mechanical properties of both nanotubes and graphene sheets have been studied extensively by computational and theoretical methods. In a sense, the study of graphene can be traced back to when Wallace (1947) reported the band structure of graphite. Sanchez-Portal et al. (1999) and Van Lier et al. (2000) determined the Young's modulus of graphene sheets with DFT and used the results to estimate the elastic properties of open and closed carbon nanotubes. Kudin et al. (2001) performed similar

* Corresponding author at: Department of Chemistry, University of Victoria, Victoria, British Columbia, Canada V8W 3V6. Tel.: +1 250 853 3264; fax: +1 250 721 7147.
E-mail address: jtpaci@uvic.ca (J.T. Paci).

0020-7683/$ - see front matter © 2012 Elsevier Ltd. All rights reserved.
http://dx.doi.org/10.1016/j.ijsolstr.2012.05.019

calculations on graphene to estimate the flexural rigidity of carbon nanotubes. Liu et al. (2007) computed the stress–strain relation of graphene under uniaxial tension by DFT computations in both the armchair and zigzag directions. Ogata and Shibutani (2003) determined the ideal tensile strength and the band structure of single-walled carbon nanotubes by DFT and tight binding methods. Dumitrica et al. (2003) studied the fracture of carbon nanotubes for a large temperature range with DFT computations. Liu et al. (2007) examined the stress–strain relation of graphene under uniaxial tension by DFT simulations, and Konstantinova et al. (2006) used similar methods to analyze the stability of the graphene structure.

The mechanical properties of nanotubes have also been studied by variants of the Cauchy-Born rule with the Tersoff-Brenner potential (Brenner, 1990, 2002). Zhao et al. (2009) studied the dependence between the size and chirality of graphene nanoribbons and their elastic properties using the AIREBO potential, which is a potential similar to Tersoff-Brenner, and a tight-binding method. Arroyo and Belytschko (2002, 2004) presented an exponential Cauchy-Born rule that accounted for the curvature of the nanotube. They studied the mechanical behavior of single layer crystalline sheets under finite deformation to simulate carbon nanotubes. Zhang et al. (2005) performed coupled molecular and continuum mechanics simulations on finite size graphene sheets with defects to estimate the fracture strength of carbon nanotubes. Huang et al. (2006b) used a Taylor series approach closely related to the Cauchy-Born rule to study the elastic properties of graphene; they made an extensive study of previously published values for Young's modulus and the role of the "thickness" of the carbon sheet on the elastic modulus. Scarpa et al. (2009) proposed a truss-type analytical model to describe the in-plane linear elastic properties of graphene.

First principles-based studies on large systems require tremendous computing power, making it prohibitively computationally expensive to simulate graphene sheets composed of more than 10,000 atoms with most types of DFT calculations. Force-field-based molecular mechanics (FF-MM) simulations of this size and larger are computationally feasible. However, the elastic properties arising from the commonly used empirical potentials for carbon, such as the Tersoff-Brenner potential, show anisotropy at small strains, and are generally inconsistent with DFT results. For example, Liu et al. (2007) showed that the tensile stress–strain behavior for different chiralities are nearly identical up to 15% strain using DFT, whereas they are distinctly different for the Tersoff-Brenner potential (Khare et al., 2008b). This inconsistency is often problematic in coupled quantum mechanical/molecular mechanical computations as discussed in Khare et al. (2007). An energy scaling scheme was presented by Khare et al. (2008a) that matches the strength obtained from FF-MM simulations to DFT results, but the approach lacks generality.

Recently several important experimental studies have made it possible to assess the adequacy of various mechanical models for graphene. Lee et al. (2008) performed nanoindentation experiments on circular graphene sheets, and obtained strikingly consistent results that suggest that defects were almost absent. They used a second order polynomial in the Green strain to fit the uniaxial stress–strain behavior of their sheets, but their polynomial was calibrated for only uniaxial tension. Peng et al. (2008) and Locascio et al. (2009) have made measurements of single-walled and multi-walled carbon nanotubes that agree quite well with the DFT calculations of Zhang et al. (2005), which have led to an increase in confidence in DFT calculations.

In this paper we present a two-dimensional anisotropic hyperelastic constitutive model calibrated using DFT calculations on a graphene unit cell. The constitutive equation is a function of two invariants of the right Cauchy–Green tensor and also the two diagonal components of the Green strain tensor. The equation consists of three parts. The first describes the mechanical behavior of compressible isotropic materials under deformations that cause small changes in area, and the second and third describe deformations involving large area changes and anisotropy. It was observed in the experiments of Tsoukleri et al. (2009) that the suspended graphene sheets buckled at about 0.7% compressive strain. It is not clear how to initiate this instability in DFT simulations. Therefore, compression behavior is not considered in the material model presented here.

Our approach is different than that of Wei et al. (2009) in which a fifth-order Taylor series of the strain energy was constructed. Our model is a modification of a standard isotropic hyperelastic work energy potential. The approach of Wei et al. represents the strain energy function as a polynomial expansion of the right-Cauchy Green tensor, while our approach bases the strain energy function on a polynomial expansion of the invariants of the right-Cauchy Green tensor and adds anisotropic terms as low order corrections. While the Wei formulation may be more accurate at very high strains, due to the larger number of parameters used, our model is significantly simpler and straight-forward to implement (Xu et al., 2012). A constitutive equation for graphene was also previously developed based on comparisons to molecular mechanics simulations (Gil et al., 2010). However, this equation is only applicable in simulations of nanoindentation experiments, whereas ours is more general. Nonlinear strain energy functions have been similarly developed for graphene nanoribbons, for which the effect of the surface energy of free edges is important (Lu et al., 2011). A general continuum description of graphene sheets based on calculations using the Tersoff-Brenner potential that accounts for in-plane and bending elasticity has also been developed (Lu and Huang, 2009).

The remainder of the paper is organized as follows. Details of the DFT calculations are given in Section 2. Section 3 describes the development of the two-dimensional anisotropic hyperelastic constitutive law. The constitutive law is then applied to a nanoindentation experiment of circular graphene sheets (Lee et al., 2008), which is presented with a numerical/experimental comparison in Section 4. Conclusions are given in Section 5.

2. DFT Studies of mechanical properties of graphene

2.1. Computational setup

DFT calculations were performed using the SIESTA computational software package (Soler et al., 2002). A Perdew–Burke–Ernzerhof (PBE) functional that uses a generalized gradient approximation (GGA) in estimating the DFT exchange–correlation term was chosen. A double-ζ plus polarization orbital (DZP) basis set was used. Carbon atoms were modeled using a Troullier–Martins pseudopotential (Troullier and Martins, 1991) with a core radius of $1.15a_0$ ($a_0 = 0.529$ Å) and a nonlinear exchange–correlation correction pseudo core radius of $1.50a_0$.

Three-dimensional periodic boundary conditions were used. We considered two unit cells: a 4-atom cluster and a 32-atom cluster (see Fig. 1). The dimension for the unit cell in Fig. 1a is $l_x = \sqrt{3}r_0$, $l_y = 3r_0$ and it is $l_x = 4\sqrt{3}r_0$, $l_y = 6r_0$ for the unit cell in Fig. 1b. r_0 indicates the length of equilibrium carbon–carbon bond in graphene. Below, we will refer to the x- and y-directions as "armchair" and "zigzag" directions, respectively. Note that different labeling conventions are sometimes used by other authors. The dimension of the unit cells along the z-direction, l_z, was chosen to eliminate spurious interactions due to the periodic boundary condition in the z-direction. A $30 \times 30 \times 1$ k-grid proved sufficient for accurately sampling the Brillouin zone for the 4-atom unit cell and an

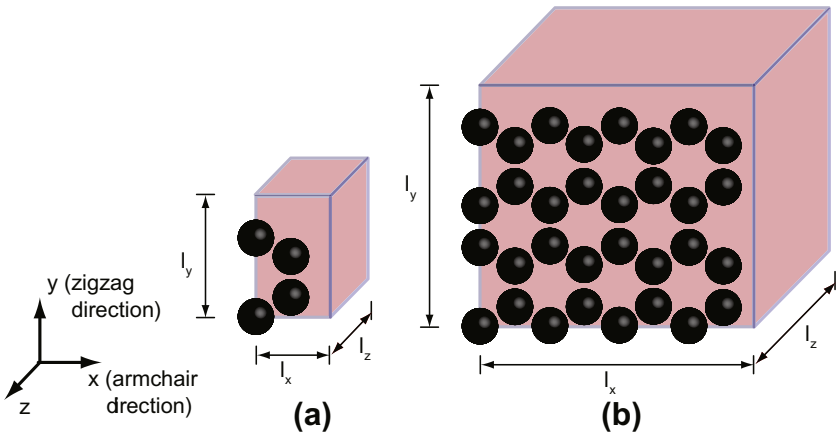

Fig. 1. The unit cells used in DFT simulations. (a) 4-atom unit cell; (b) 32-atom unit cell.

$8 \times 15 \times 1$ k-grid for the 32-atom unit cell. A conjugate gradient solver was used for geometry optimization. All the results were for 0 K and electron spin polarization was not allowed.

In computing the Young's modulus of graphene, it is common to use 3.4 Å (Baskin and Meyer, 1955), the interlayer distance of graphite sheets, as the thickness, which is denoted by h. In our treatment, we assume that this thickness is independent of load. The stresses output by SIESTA were scaled by $\alpha = l_z/h$ to calculate the equivalent stresses, σ^e_{ij}, on surfaces with thickness h, which are

$$\sigma^e_{ij} = \alpha\sigma_{ij} \quad i,j = 1,2 \tag{1}$$

where σ_{ij} is the stress on the unit-cell wall output by SIESTA.

The stress tolerance used was 0.1 GPa, so the maximum uncertainty of the normalized stress is $\frac{\alpha}{10}$ GPa. The use of smaller stress tolerances makes calculations more computationally demanding. Because both the stress tolerance and the computational cost are proportional to the length of the unit cell along the z axis, l_z was chosen such that it was just large enough to avoid any spurious interaction along the z-direction. We tested $l_z = 60$ Å, 30 Å, 10 Å, 5 Å. It turned out that 10 Å was the best choice among the four. Both 60 Å and 30 Å have a higher computation cost and 5 Å does not eliminate spurious interactions. Smaller stress tolerances were considered but they require much more computational time and can lead to unphysical results. For example, with a very small stress tolerance, l_z converges to 5.4 Å, which is not consistent with experimental observations (Baskin and Meyer, 1955). The reason for this is that the graphene layers interact by van der Waals forces, which PBE/DZP does not represent accurately; PBE was designed to describe covalent bond interactions which are much stronger. The equilibrium C–C bond length in graphene lattice was found by geometry optimization to be 1.43 Å.

Variable cell PBE/DZP computations with stress boundary conditions, which correspond to uniaxial tension along the zigzag and armchair directions were performed. Under uniaxial tension, only one stress component was non-zero, which was the normal stress on the surface where the tensile load was applied. The stress increment was 1 GPa. The computations failed to converge when the modulus of graphene sheet became negative (strain softening). Therefore, a displacement boundary condition was used instead at the onset of strain softening. We also computed the material response for graphene under equal biaxial stretching. Displacement boundary conditions were used and the stretches in both the armchair and zigzag directions were enforced to be the same.

2.2. Results and discussion

The DFT results for 4- and 32-atom unit cells are identical. This suggests that graphene can be homogenized using such small unit cells, although we did not perform an exhaustive examination of this issue. The stress–strain curves when the sheet is under uniaxial tension along the zigzag and armchair directions are shown in Fig. 2a. The results are presented in terms of the Cauchy (physical) stress, $\boldsymbol{\sigma}$, the principal stretch, λ_i, $i = 1,2$, and the engineering strain, ϵ_i. The strain is related to the principal stretch by

$$\epsilon_i = \lambda_i - 1 = \frac{l_i}{l_i^0} - 1 = \frac{l_i - l_i^0}{l_i^0}, \tag{2}$$

where l_i^0 is the length of the undeformed unit cell along the ith dimension and l_i is the length of the deformed, stressed unit cell. Some of the results are presented in terms of the deformation gradient, $\mathbf{F} = \partial\phi/\partial\mathbf{X}$, where ϕ is the motion and $\mathbf{X} = \{X, Y, Z\}$ are the vectors of material coordinates. Equivalently, $\mathbf{F} = \partial\mathbf{x}/\partial\mathbf{X}$, where $\mathbf{x} = \phi(\mathbf{X})$.

The material response of graphene under tensile stress obtained by DFT computations are shown in Fig. 2. It can be seen in panel a that, for a thickness of 3.4 Å, the maximum tensile stresses are 107.2 GPa and 117.5 GPa for the zigzag and armchair directions, respectively. The corresponding stretch at the maxima of the stresses are 1.20 and 1.25. The maximum stresses are very close to the onset of the phonon instability as calculated by Liu et al. (2007). It is also shown in Fig. 2a that the mechanical response of the graphene sheet under uniaxial tension is almost linear until 10% strain. Subsequently it deviates significantly from linearity. For example, the slope of the curve at zero strain is four times greater than at 15% strain. It also can be seen that the stress–strain curves of the graphene sheet in the armchair and zigzag directions are almost identical until the engineering strain is about 15%. Thus for small strain the material is nearly isotropic. Anisotropy develops at moderate stretch. At approximately 15% strain, the zigzag stiffness rapidly decreases to zero, whereas in the armchair direction, the stiffness is maintained much longer. For equal biaxial stretching, the mechanical behavior of the armchair and zigzag directions are identical (see Fig. 2b). No anisotropy was observed under equal biaxial stretching, a finding consistent with the maintained hexagonal symmetry of the system for this case. It is then reasonable to treat graphene as an isotropic material for biaxial strain and small uniaxial tensile strain.

To compare DFT and molecular mechanics (MM) methods, the MM results for the Tersoff-Brenner potential (Brenner et al., 2002) are also shown in Fig. 2. The curves from MM calculations terminate when instability occurs, which may be caused by defect

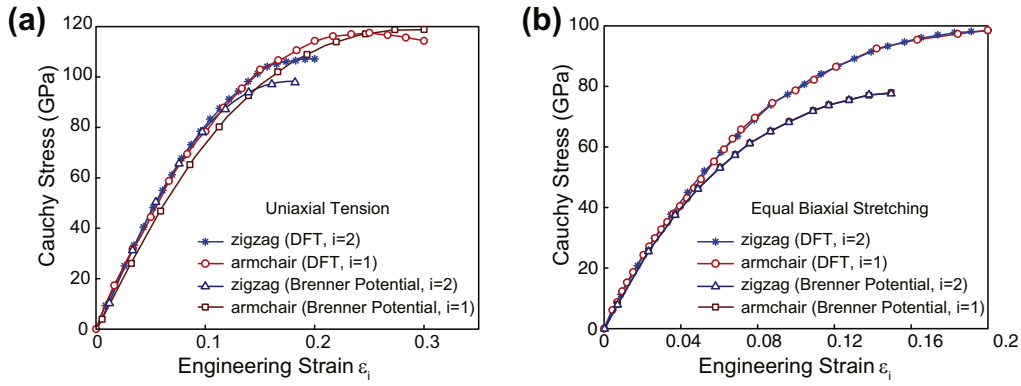

Fig. 2. Material response calculated by DFT and MM for the graphene sheet under (a) uniaxial tension along zigzag and armchair directions; (b) equal biaxial stretching.

nucleation. Fig. 2a shows that the graphene sheet has different stiffnesses along the zigzag and armchair directions and the tensile strength differs by 5–10% from the DFT results depending on the loading direction. The orthotropicity of the Tersoff-Brenner-based predictions of the type shown in Fig. 2a has been previously reported (Reddy et al., 2006; Lu et al., 2011). It also can be seen in Fig. 2b, that the slope of the equal biaxial stretching curve at small strains from MM calculations is smaller than the DFT results, and therefore the stresses predicted in biaxial tension are significantly lower than those for DFT.

3. Proposed constitutive law for graphene

Graphene at room temperature and below appears to exhibit perfectly reversible mechanical behavior. There is evidence that at high temperatures ($T > 2000^{\circ}C$) (Huang et al., 2006a), the response is plastic, which is characterized by Stone–Wales dislocations as described by Ding et al. (2007)). However, the activation temperature for these dislocations is quite high, so they can probably be ignored for constitutive models in the range $T \sim 0$—400 K. Therefore, we have chosen a hyperelastic constitutive equation for graphene. Based on the observation in the previous section, we developed a two-dimensional anisotropic hyperelastic law. Only the material behavior under tensile stresses is considered, because the graphene sheet buckles under compression (Tsoukleri et al., 2009). The strain energy density function is a function of the principal invariants, (I_1, I_2), of the right Cauchy–Green tensor, $\mathbf{C}$, and the diagonal components of the Green strain, (E_{11}, E_{22}). The first principle invariant $I_1 = \mathrm{tr}(\mathbf{C}) = C_{11} + C_{22}$, and the second principle invariant $I_2 = \det(\mathbf{C})$, where C_{11} and C_{22} are the principal values of the Right-Cauchy Green deformation tensor. The deformation gradient, $\mathbf{F}$, and the Green strain, $\mathbf{E}$, tensors are related to the right Cauchy–Green tensor by $\mathbf{C} = \mathbf{F}^{\mathrm{T}}\mathbf{F} = 2\mathbf{E} + \mathbf{I}$, where $\mathbf{I}$ is the identity tensor.

The potential reads

$$w(I_1, I_2, E_{11}, E_{22}) = \sum_{i=1}^{N_1} c_i (I_1 - 2)^i + \sum_{k=1}^{N_2} d_k (\ln J)^{2k} - 2\sum_{i=1}^{N_1} c_i (\ln J)^i + \sum_{l=1}^{5} a_l f_l(E_{11}, E_{22})(J - b_l)[\ln(J - b_l)]^3 \quad (3)$$

where c_i, d_k, and a_l are the fitting coefficients, and $J = \det(\mathbf{F}) = \sqrt{I_2}$. N_1 and N_2 are the number of polynomial terms in the constitutive equation. They can be adjusted to find the optimal fit. The definitions of the functions, f_i, are

$$b_1 = 0.05, \quad b_2 = 0.15, \quad b_3' = 0.07, \quad b_4' = 0.09, \quad b_5' = 0.12 \quad (4)$$

$$f_1 = H\left(E_{22} - \frac{b_1}{2}\right) H\left(E_{11} - \frac{b_1}{2}\right) \quad (5)$$

$$f_2 = H\left(E_{22} - \frac{b_2}{2}\right) H\left(E_{11} - \frac{b_2}{2}\right) \quad (6)$$

$$f_j = H\left(E_{22} - b_j'\right) H(-E_{11}) \quad j = 3, 4, 5 \quad (7)$$

$$b_j = \sqrt{2b_j' + 1}\left[1 - v\left(\sqrt{2b_j' + 1} - 1\right)\right] - 1 \quad j = 3, 4, 5 \quad (8)$$

where $H(\bullet)$ is the Heaviside function, b_j are the threshold values in strain where the anisotropic terms are activated, and v is the Poisson's ratio which will be discussed later in this section. The terms in Eqs. (5)–(7) account for the anisotropy.

The constants, c_i and d_k, were determined using the uniaxial tension results for the armchair direction. When the coefficients obtained were applied to biaxial stretching, the fitted stress–strain curve started to deviate from the DFT results at $J \sim 1.05$. Therefore, the a_1 and a_2 terms were added to obtain a good fit for biaxial stretching. The a_3 to a_5 terms account for the anisotropy under uniaxial tension. The exponents of these terms were chosen such that the terms do not introduce discontinuities in the resulting stresses and tangent stiffnesses. There are other options for the a_3 to a_5 terms. For example, instead of I_2, the first principal invariant, I_1, could be used as the variable.

The second Piola–Kirchhoff (PK2) stress tensor $\mathbf{S}$ of a hyperelastic material can be obtained by taking the derivative of the strain energy density, w, with respect to $\mathbf{C}$, so

$$\mathbf{S} = 2\frac{\partial w}{\partial \mathbf{C}} = 2\left(\frac{\partial w}{\partial I_1}\frac{\partial I_1}{\partial \mathbf{C}} + \frac{\partial w}{\partial I_2}\frac{\partial I_2}{\partial \mathbf{C}} + \frac{\partial w}{\partial E_{11}}\frac{\partial E_{11}}{\partial \mathbf{C}} + \frac{\partial w}{\partial E_{22}}\frac{\partial E_{22}}{\partial \mathbf{C}}\right) \quad (9)$$

The last two terms varnish because $\frac{\partial w}{\partial E_{11}} = \frac{\partial w}{\partial E_{22}} = 0$. The derivatives of the invariants with respect to the right Cauchy–Green tensor are given in Belystchko et al. (2001). They are

$$\frac{\partial I_1}{\partial \mathbf{C}} = \mathbf{I} \quad (10)$$

and

$$\frac{\partial I_2}{\partial \mathbf{C}} = I_2 \mathbf{C}^{-1} \quad (11)$$

The relation between the PK2 stress and the Cauchy stress $\boldsymbol{\sigma}$ is given by

$$\boldsymbol{\sigma} = J^{-1}\mathbf{F}\mathbf{S}\mathbf{F}^{\mathrm{T}} = 2J^{-1}\left(\frac{\partial w}{\partial I_1}\mathbf{B} + I_2\frac{\partial w}{\partial I_2}\mathbf{I}\right) \quad (12)$$

where $\mathbf{B} = \mathbf{F}\mathbf{F}^{\mathrm{T}}$ is the left Cauchy–Green tensor.

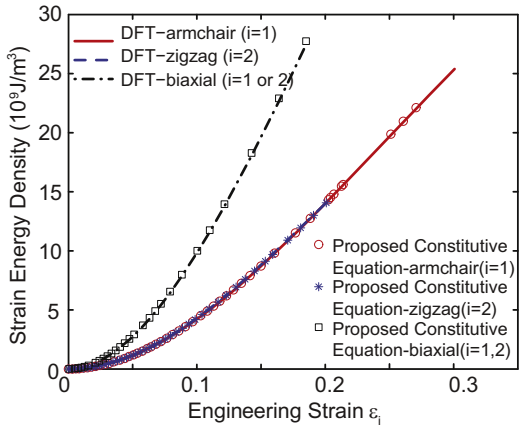

Fig. 3. Strain energy densities from the proposed constitutive equation for graphene under uniaxial tension along the armchair and zigzag directions, and under equal biaxial stretching, compared to DFT results.

The tangent modulus is related to the second derivative of the strain energy density with respect to the right Cauchy–Green tensor, i.e.,

$$\mathcal{C}^{SE} = 4\frac{\partial^2 w}{\partial \mathbf{C}\partial \mathbf{C}} \tag{13}$$

or in component form

$$\frac{1}{4}\mathcal{C}^{SE}_{ijkl} = \frac{\partial^2 w}{\partial I_1^2}\delta_{ij}\delta_{kl} + \left(\frac{\partial^2 w}{\partial I_2^2}I_2^2 + \frac{\partial w}{\partial I_2}I_2\right)\left(C^{-1}\right)_{ij}\left(C^{-1}\right)_{kl} - \frac{1}{2} \times \frac{\partial w}{\partial I_2}I_2\left(\left(C^{-1}\right)_{ik}\left(C^{-1}\right)_{jl} + \left(C^{-1}\right)_{il}\left(C^{-1}\right)_{jk}\right) \tag{14}$$

The tangent modules $\mathcal{C}^{SE}$ relates PK2 to the Green strain by

$$d\mathbf{S} = \mathcal{C}^{SE} d\mathbf{E} \tag{15}$$

The relationship between the stress invariants and the principal stretch ratios are

$$I_1 = \lambda_1^2 + \lambda_2^2 \tag{16}$$

and

$$I_2 = \lambda_1^2\lambda_2^2 = J^2 \tag{17}$$

Under uniaxial tension, the deformation gradient can be written as

$$\mathbf{F} = \begin{bmatrix} \lambda_1 & 0 \\ 0 & \lambda_2 \end{bmatrix} \tag{18}$$

Table 1
Coefficients in Eq. (3) of the proposed hyperelastic constitutive model for graphene.

i	1	2	3	4	5
c_i (GPa)	210.75	−98.72	6.91	–	–
d_i (GPa)	307.87	237.26	–	–	–
a_i (GPa)	30.00	−51.67	833.33	−2000.00	1000.00

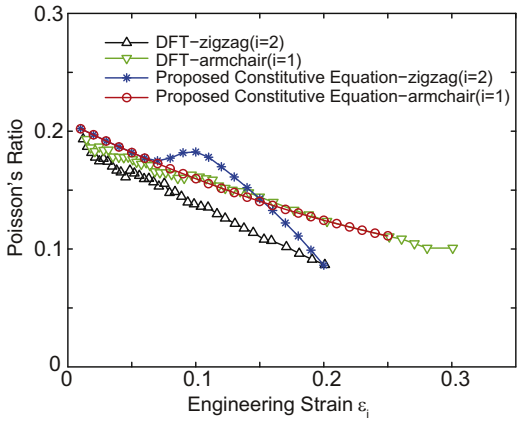

Fig. 5. Poisson's ratios from the proposed constitutive equation for graphene under uniaxial tension along the armchair and zigzag directions, compared to DFT results.

Our energy criterion is independent of deformation in the sheet thickness direction. Substituting Eqs. (18) and (3) into Eq. (12) gives equations for the Cauchy stress components

$$\sigma_1 = 2J^{-1}\sum_{i=1}^{N_1} i c_i (I_1-2)^{i-1}\lambda_1^2 + 2J^{-1}\sum_{k=1}^{N_2} k d_k (\ln J)^{2k-1} - 2J^{-1}\sum_{i=1}^{N_1} i c_i (\ln J)^{i-1} + \sum_{l=1}^{5} a_l f_l [\ln(J-b_l)]^3 + 3\sum_{l=1}^{5} a_l f_l [\ln(J-b_l)]^2 \tag{19}$$

$$\sigma_2 = 2J^{-1}\sum_{i=1}^{N_1} i c_i (I_1-2)^{i-1}\lambda_2^2 + 2J^{-1}\sum_{k=1}^{N_2} k d_k (\ln J)^{2k-1} - 2J^{-1}\sum_{i=1}^{N_1} i c_i (\ln J)^{i-1} + \sum_{l=1}^{5} a_l f_l [\ln(J-b_l)]^3 + 3\sum_{l=1}^{5} a_l f_l [\ln(J-b_l)]^2 \tag{20}$$

The fitting procedure is similar to the one described in Oswald et al. (2007). We first fit the terms with the DFT results for the graphene unit cell under uniaxial tension along the armchair direction. The last term in Eq. (20) vanishes because E_{22} is negative when the graphene sheet is under uniaxial tension along the armchair

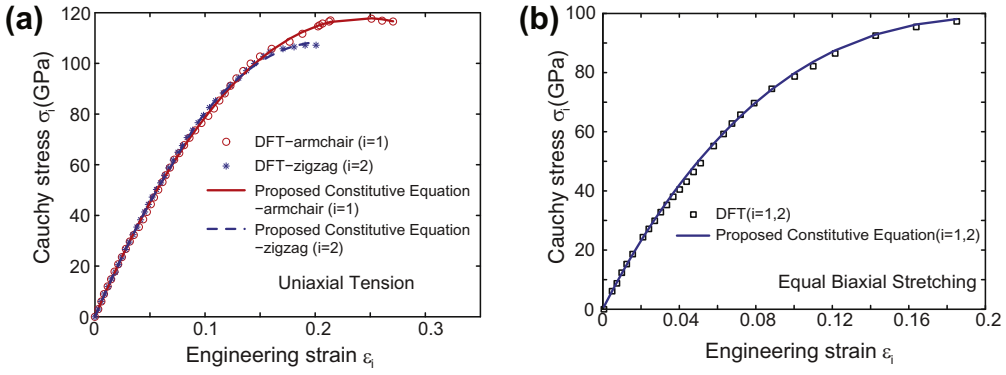

Fig. 4. Results from the proposed constitutive equation for graphene under (a) uniaxial tension along armchair and zigzag directions, and (b) equal biaxial stretching, compared to DFT results.

Table 2
The elastic constants of graphene and the strain at onset of material softening from the proposed hyperelastic constitutive law and the literature.

	Young's Modulus (TPa)	Poisson's ratio	Stretch at σ_{max}
Hyperelastic model	1.030	0.221	1.19(zigzag)1.24 (armchair)
DFT by Kudin et al. (2001)	1.015	0.149	–
DFT by Liu et al. (2007)	1.034	0.186	1.19 (zigzag)1.27 (armchair)
Experiment by Lee et al. (2008)	0.853–1.147	–	1.25
MM by Arroyo and Belytschko (2004) with Brenner as given in Brenner (1990)	0.715	0.397	–
Experiment* by Peng et al. (2008)	1.057	–	1.12
Tight binding* by Ogata and Shibutani (2003)	0.972	–	1.20
Coupled MM/CM* by Zhang et al. (2005)	0.859	–	1.18 (zigzag) 1.30 (armchair)
DFT* by Sanchez-Portal et al. (1999)	1.800	–	1.19 (zigzag)1.14 (armchair)
Coupled QM/MM** by Khare et al. (2007)	1.049	—	1.12 (zigzag)

*Obtained from the reported stress–strain curves of carbon nanotubes. **Obtained from the stress–strain curve of graphene with a one-atom vacancy.

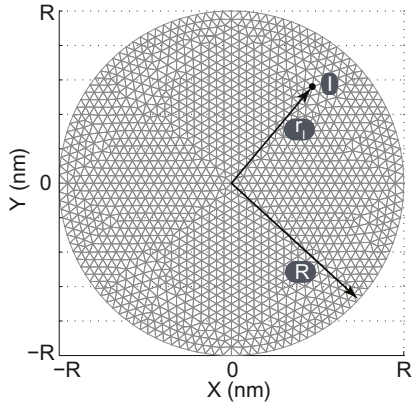

Fig. 6. A sketch of the finite element mesh of a circular graphene sheet of radius, R. r_I indicates the distance between node I and the center of the membrane.

direction. A function of only c_k can be obtained by subtracting Eq. (20) from Eq. (19), which gives

$$\sigma_1 - \sigma_2 = 2A\sum_{i=1}^{N_1} i c_i B^{i-1} \tag{21}$$

where $A = J^{-1}(\lambda_1^2 - \lambda_2^2)$, and $B = I_1 - 2$. A least-squares fit with $N_1 = 3$ was used to determine the coefficients c_i.

To fit the PBE/DZP results, a residual, r, was defined as

$$r = \sum_j \left(P_j - P_j^{\text{fit}}\right)^2 \tag{22}$$

where j ranges from 1 to the number of load steps in the PBE/DZP computations, P_j are the PBE/DZP results for different strains and P_j^{fit} are the corresponding values computed from Eq. (21). The fitting coefficients were obtained by setting the derivatives of r with respect to the fitting coefficients to zero, i.e.,

$$\frac{\partial r}{\partial c_k} = 2\sum_j \left(P_j - 2A_j \sum_{i=1}^{N_1} i c_i B_j^{i-1}\right) A_j k B_j^{k-1} = 0 \quad k = 1, \ldots, N_1 \tag{23}$$

After substituting the c_k, where $k = 1, \ldots, N_1$, thus obtained into Eq. (19), d_k, where $k = 1, \ldots, N_2$, were found in an analogous way. For $N_1 = 3$ and $N_2 = 2$, the fitted constitutive equation shows good agreement with the PBE/DZP results.

The coefficients a_1 and a_2 were determined from the biaxial stretching results, and a_3 through a_5 were calibrated using the difference in the tensile stresses between the uniaxial tensions along the zigzag and armchair directions. The fitted strain energy densities are shown in Fig. 3, and are compared to the energy densities from the DFT calculations. The resulting stress–strain relations are shown in Fig. 4, along with the DFT results. Very good agreement was obtained in all cases. The fitting coefficients are listed in Table 1.

Poisson's ratios in the armchair and zigzag directions are compared between the DFT results and the proposed constitutive model in Fig. 5. The ratios were calculated by finding the transverse strain that made the stress state uniaxial. The curves for the armchair direction are almost identical. The Poisson's ratio curve for the zigzag direction from the constitutive equation takes an unrealistic bend away and then back toward the DFT results at strains larger than $\sim 7\%$. This behavior is due to a limitation of this equation for predicting this response accurately for these strains. At very small strains, the DFT results are inaccurate due to the stress tolerance of 0.1 GPa. For example, an uniaxial engineering strain of 0.3% in the armchair direction generates a tensile stress of 1 GPa, however the transverse stress generated by this uniaxial strain is less than 0.1 GPa. Therefore, the resulting Poisson's ratios from PBE/DZP calculations are not accurate at very small strains, so we did not report them in the figure.

The elastic constants of graphene can be calculated using the coefficients from Table 1; the shear modulus is $\mu = 2c_1 = 421.5$ GPa, the Lamé constant $K = 2d_1 = 615.74$ GPa, Young's modulus is $Y = \frac{9K\mu}{3K+\mu} = 1.030$ TPa, and Poisson's ratio is $\nu = \frac{3K-2\mu}{2(3K+\mu)} = 0.22$. The elastic constants of graphene and the strain at onset of material softening from the proposed constitutive equation are compared to values from the literature in Table 2. Literature-reported results for carbon nanotubes are also shown. It can be seen that the mechanical properties from the continuum model match the various DFT-based results better than those predicted using empirical potentials.

4. Indentation example

To test the effectiveness of this constitutive model, we consider the nanoindentation experiment of Lee et al. (2008). In their experiment, graphene sheets of radius 500 nm and 750 nm were indented in the center to various indentation depths, d, and the force–deflection relations were obtained to evaluate the elastic constants. We simulated the experiments numerically. A simple in-house total Lagrangian-based nonlinear static finite element code was used. A sketch of the finite element model is shown in Fig. 6. The graphene sheet of radius R consists of 1495 nodes and 2864 linear triangular membrane elements. The boundary of a sheet was fixed ($u_x = u_y = u_z = 0\ \forall X, Y \in \{X^2 + Y^2 = R^2\}$), and the center node was displaced by d. Lee et al. showed that the load–deflection curves are not sensitive to the indenter size, except that it was easier to break the sheets with smaller indenters.

The simulated load–deflection curves with $R = 500$ nm and $R = 750$ nm are shown in Fig. 7, with the experimental data. Excellent agreement was obtained. The simulation curves terminate where the numerical computations failed to converge. The terminations may indicate the fracture loads. This will be investigated in subsequent work, where the importance of bending stiffness will also be explored. For the $R = 500$ nm model, the breaking force was 1567 nN and the maximum deflection was 110 nm. They are 2188 nN and 160 nm for the $R = 750$ nm sheet. The breaking

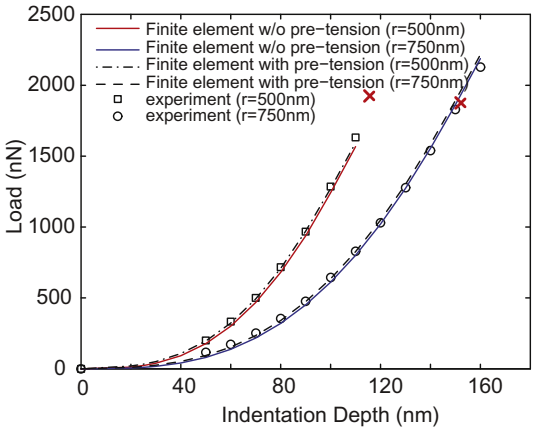

Fig. 7. The relationships between the vertical reaction force at the center node and the indentation depths, in simulations with and without (w/o) pre-tension, compared to the experimental results of Lee et al. (2008). The red X's mark the experimental fracture loads, with an indenter of radius 16.5 nm.

points in the experiments using an indenter with a tip-radius of 16.5 nm are marked with red X's in the figure. The corresponding fracture loads are 1905 nN and 1868 nN for the 500 nm and 750 nm graphene sheets, respectively. In the experiment, the breaking forces were higher with an indenter tip of larger radius.

Pre-tension in the radial direction is considered in the experiments of Lee et al. (2008). Computed results with pre-tension are also shown in Fig. 7. We considered 0.2 nm pre-stretch in radius, which corresponds to 0.14 N/m and 0.09 N/m pre-tensions on the $R = 500$ nm and $R = 750$ nm sheets, respectively. The difference between the load–deflection curves with and without pre-tension is almost negligible at large deflections. However, its effect is more important at small deflections. The change in the reaction force at the center node due to pre-tension is greater than 60% for 20 nm deflection. The pre-tension effect decreases drastically with the indentation depth. For 100 nm indentation, the change in reaction force caused by pre-tension is only 1%.

5. Conclusions

The material response of graphene under uniaxial and equal biaxial stretching was computed with the DFT method PBE/DZP. A two-dimensional anisotropic hyperelastic model was developed from the PBE/DZP results by applying a least-squares fit. The resulting constitutive law is a function of two principal invariants of the right Cauchy–Green tensor and two diagonal components of the Green strain tensor. The law accounts for the anisotropy at large uniaxial tensile strain. The elastic constants of the presented model are as accurate as the DFT computations and the model reproduces the PBE/DZP results very well. Nanoindentation of circular graphene sheets was simulated using the proposed law, with and without considering pre-tension. The numerical results show very good agreement with experimental data. The effect of pre-tension was shown to be not significant except at very small strains. This development of an accurate continuum model can facilitate mechanical behavior studies of graphene sheets.

Acknowledgment

We gratefully acknowledge grant support from the Office of Naval Research under Grant No. N00014–08-1–1191 and the Army Research Office under Grant No. W911NF-08–1-212.

References

Arroyo, M., Belytschko, T., 2002. An atomistic-based finite deformation membrane for single layer crystalline films. J. Mech. Phys. Solids 50, 1941–1977.
Arroyo, M., Belytschko, T., 2004. Finite element methods for the non-linear mechanics of crystalline sheets and nanotubes. Int. J. Numer. Methods Eng. 59, 419–456.
Baskin, Y., Meyer, L., 1955. Lattice constants of graphite at low temperatures. Phys. Rev. 100, 544.
Belystchko, T., Liu, W.K., Moran, B., 2001. Nonlinear Finite Elements for Continua and Structures. John Wiley & Sons Ltd.
Brenner, D.W., 1990. Empirical potential for hydrocarbons for use in simulating the chemical vapor deposition of diamond films. Phys. Rev. B 42, 9458–9471.
Brenner, D.W., Shenderova, O.A., Harrison, J.A., Stuart, S.J., Ni, B., Sinnott, S.B., 2002. A second-generation reactive empirical bond order (REBO) potential energy expression for hydrocarbons. J. Phys.: Condens. Mat. 14, 783–802.
Ding, F., Jiao, K., Wu, M., Yakobson, B., 2007. Pseudoclimb and dislocation dynamics in superplastic nanotubes. Phys. Rev. Lett. 98, 75503.
Dumitrica, T., Belytschko, T., Yakobson, B.I., 2003. Bond–breaking bifurcaion states in carbon nanotube fracture. J. Chem. Phys. 118, 9485–9488.
Frank, I., Tanenbaum, D., Van der Zande, A., McEuen, P., 2007. Mechanical properties of suspended graphene sheets. J. Vac. Sci. Technol. B 25, 2558–2561.
Geim, A., Novoselov, K., 2007. The rise of graphene. Nature Mater. 6, 183–191.
Gil, A.J., Adhikari, A., Scarpa, F., Bonet, J., 2010. The formation of wrinkles in single-layer graphene sheets under nanoindentation. J. Phys.: Condens. Mat. 22, 145302.
Huang, J., Chen, S., Wang, Z., Kempa, K., Wang, Y., Jo, S., Chen, G., Dresselhaus, M., Ren, Z., 2006a. Superplastic carbon nanotubes. Nature 439, 281.
Huang, Y., Wu, J., Hwang, K., 2006b. Thickness of graphene and single-wall carbon nanotubes. Phys. Rev. B 74, 245–413.
Khare, R., Mielke, S.L., Paci, J.T., Schatz, G.C., Belytschko, T., 2008a. A simple energy-scaling scheme for fine-tuning empirical potentials for coupled quantum mechanical/molecular mechanical studies. Chem. Phys. Lett. 460, 311–314.
Khare, R., Mielke, S.L., Paci, J.T., Zhang, S.L., Ballarini, R., Schatz, G.C., Belytschko, T., 2007. Coupled quantum mechanical/molecular mechanical modeling of the fracture of defective carbon nanotubes and graphene sheets. Phys. Rev. B 75, 075–412.
Khare, R., Mielke, S.L., Schatz, G.C., Belytschko, T., 2008b. Multiscale coupling schemes spanning the quantum mechanical, atomistic forcefield, and continuum regimes. Comput. Methods Appl. Mech. Eng. 197, 3190–3202.
Konstantinova, E., Dantas, S., Barone, P., 2006. Electric and elastic properties of two-dimensional carbon planes. Phys. Rev. B 74, 035417.
Kudin, K., Scuseria, G., Yakobson, B., 2001. C_2F, BN and C nanoshell elasticity from ab initio computations. Phys. Rev. B 64, 235406.
Lee, C., Wei, X., Kysar, J., Hone, J., 2008. Measurement of the elastic properties and intrinsic strength of monolayer graphene. Science 321, 385–388.
Li, X., Wang, X., Zhang, L., Lee, S., Dai, H., 2008. Chemically derived, ultrasmooth graphene nanoribbon semiconductors. Science 319, 1229.
Liu, F.P.M., Li, J., 2007. Ab initio calculation of ideal strength and phonon instability of graphene under tension. Phys. Rev. B 76, 064120.
Locascio, M., Peng, B., Zapol, P., Zhu, Y., Li, S., Belytschko, T., Espinosa, H.D., 2009. Tailoring the load carrying capacity of MWCNTs through inter-shell atomic bridging. Exp. Mech. 49, 169–182.
Lu, Q., Gao, W., Huang, R., 2011. Atomistic simulation and continuum modeling of graphene nanoribbons under uniaxial tension. Modell. Simul. Mater. Sci. Eng. 19, 054006.
Lu, Q., Huang, R., 2009. Nonlinear mechanics of single-atomic-layer graphene sheets. Int. J. Appl. Mech. 1, 443.
Lu, X., Yu, M., Huang, H., Ruoff, R.S., 1999. Tailoring graphite with the goal of achieving single sheets. Nanotechnology 10, 269.
Mermin, N., 1968. Crystalline order in two dimensions. Phys. Rev. 176, 250–254.
Novoselov, K., Jiang, D., Schedin, F., Booth, T., Khotkevich, V., Morozov, S., Geim, A., 2005. Two-dimensional atomic crystals. PNAS 102, 10451–10453.
Ogata, S., Shibutani, Y., 2003. Ideal tensile strength and band gap of single-walled carbon nanotubes. Phys. Rev. B 68, 165–409.
Ohta, T., Bostwick, A., Seyller, T., Hom, K., Rotenberg, E., 2006. Controlling the electronic structure of bilayer graphene. Science 313, 951–954.
Oswald, J., Daniels, C., Steinetz, B., Dunlap, P., 2007. Simulating elastomer seal mechanics for a low impact docking system. In: AIAA SPACE 2007 Conference & Exposition. American Institute of Aeronautics and Astronautics.
Paci, J.T., Belytschko, T., Schatz, G.C., 2007. Computational studies of the structure, behavior upon heating, and mechanical properties of graphite oxide. J. Phys. Chem. 111, 18099–18111.
Peng, B., Locascio, M., Zapol, P., Li, S., Mielke, S.L., Schatz, G.C., Espinosa, H.D., 2008. Measurements of near-ultimate strength for multiwalled carbon nanotubes and irradiation-induced crosslinking improvements. Nature Nanotechnol. 3, 626–631.
Reddy, C.D., Rajendran, S., Liew, K.M., 2006. Equilibrium configuration and continuum elastic properties of finite sized graphene. Nanotechnology 17, 864–870.
Sakhaee-Pour, A., Ahmadian, M., Vafai, A., 2008. Potential application of single-layered graphene sheet as strain sensor. Solid State Commun. 147, 336–340.
Sanchez-Portal, D., Artacho, E., Soler, J., Rubio, A., Ordejon, P., 1999. Ab initio structrual, elastic, and vibrational properties of carbon nanotubes. Phys. Rev. B 59, 12678.

Scarpa, F., Adhikari, S., Phani, S., 2009. Effective elastic mechanical properties of single layer graphene sheets. Nanotechology 20, 065709.
Shioyama, H., 2001. Cleavage of graphite to graphene. J. Mater. Sci. Lett. 20, 499–500.
Soler, J.M., Artacho, E., Gale, J.D., García, A., Junquera, J., Ordejón, P., Sánchez-Portal, D., 2002. The SIESTA method for ab initio order-N materials simulation. J. Phys.: Condens. Mat. 14, 2745–2779.
Stankovich, S.S., Dikin, D.A., Dommett, G., Kohlhaas, K.M., Zimney, E.J., Stach, E.A., Piner, R.D., Nguyen, S.T., Ruoff, R.S., 2006. Graphene-based composite materials. Nature 442, 282–286.
Stoller, M.D., Park, S., Zhu, Y., An, J., Ruoff, R.S., 2008. Graphene-based ultracapacitors. Nano Lett. 8, 3498–3502.
Troullier, N., Martins, J., 1991. Efficient pseudopotentials for plane-wave calculations. Phys. Rev. B 43, 1993–2006.
Tsoukleri, G., Parthenios, J., Papagelis, K., Jalil, R., Ferrari, A., Geim, A., Novoselov, K., Galiotis, C., 2009. Subjecting a graphene monolayer to tension and compression. Small 5, 2397–2402.
Van Lier, G., Van Alsenoy, C., Van Doren, V., Geerlings, P., 2000. Ab initio study of the elastic properties of single-walled carbon nanotubes and graphene. Chem. Phys. Lett. 326, 181–185.
Wallace, P., 1947. The band theory of graphite. Phys. Rev. 71, 622–634.
Wei, X., Fragneaud, B., Marianetti, C.A., Kysar, J.W., 2009. Nonlinear elastic behavior of graphene: Ab initio calculations to continuum description. Phys. Rev. B 80, 205407.
Xu, M., Tabarraei, A., Paci, J.T., Oswald, J., Belytschko, T., 2012. A coupled quantum/continuum mechanics study of graphene fracture. Int. J. Frac. 173, 163–171.
Zhang, S., Mielke, S.L., Khare, R., Troya, D., Ruoff, R.S., Schatz, G.C., Belytschko, T., 2005. Mechanics of defects in carbon nanotubes: atomistic and multiscale simulations. Phys. Rev. B 71, 115403.
Zhao, H., Min, K., Aluru, N., 2009. Size and chirality dependent elastic properties of graphene nanoribbons under uniaxial tension. Nano Lett. 9, 3012–3015.